Cooperative radiative decay of disordered molecular monolayers

Ningjun Wang,* Vladimir Chernyak,† and Shaul Mukamel
Center for Photoinduced Charge Transfer, Department of Chemistry, University of Rochester, Rochester, New York 14627
(Received 2 May 1994)

The time-resolved spontaneous emission from a disordered molecular monolayer is calculated using Green-function techniques. In addition to a fast-decaying transmitted and reflected coherent component in the forward direction, and a slowly decaying, incoherent, spatially homogeneous background, we predict a backscattering peak related to weak localization of excitons. Analytical and numerical calculations of the energy- and disorder-dependent cooperative radiative decay rate, the quantum yield of the coherent and incoherent components, and the exciton diffusion coefficient are presented.

I. INTRODUCTION

Radiative dynamics of molecular aggregates is an area of intense current interest.[1-7] In three-dimensional crystals, the radiation modes and the polarization of the material system combine to form new normal modes (polaritons) which show no radiative decay.[8-11] However, geometrically confined systems such as two-dimensional crystals do have radiative decay since photons created in the material system can escape.[12] Effects of radiative decay in the linear[13] as well as the nonlinear[14-17] optical response were considered. The fluorescence decay may be characterized by cooperative spontaneous emission and the aggregate decay rate is $N_{eff}\gamma_0$, with γ_0 being the radiative decay rate of a single molecule, and N_{eff} being the characteristic coherence size. The concept of a radiative coherence size was advanced by Mobius and Kuhn[2] in analyzing the dependence of fluorescence quenching on the acceptor surface density for a system consisting of an acceptor monolayer on top of a J-aggregate monolayer. The role of disorder on the radiative coherence size has been addressed in recent experiments involving mixed monolayers of cyanine dyes (J-aggregates).[4-7] Disordered aggregates are characterized by several coherence sizes such as the mean free path connected with exciton elastic or inelastic scattering, and their effect on the radiative decay should lead to some clear signatures in the optical response. In particular, scattering on impurities can lead to the population of exciton states that are "dark" in an ideal system. These states have long radiative lifetimes since they cannot emit directly, and need to be scattered again to become "bright" and emit a photon. This should result in a substantial increase of the emission time scale of the incoherent component in time-resolved fluorescence experiments.

In a recent study,[18] the time-resolved spontaneous emission signal of a two-dimensional molecular aggregate with topological disorder, was calculated using a quantum description of the radiation field, and expressed in terms of the disorder averaged particle-hole (p-h) Green function. Using the ladder diagram approximation for this Green function, the photon emission rate was found to consist of a fast (coherent) component and a slow (incoherent) component. The frequency-dependent radia-

tive decay rate for aggregates with physical size much smaller than the optical wavelength was calculated numerically. In an ideal two-dimensional monolayer, the bright excited states, whose momenta are smaller than the optical wave vector $k_0 \equiv \Omega/c$, occupy a very small region in the exciton band. In disordered aggregates, dark excitons (with momentum larger than k_0) become weakly bright due to exciton scattering, and they have long radiative lifetimes.

In the present paper, we extend this work in several respects. First, we consider a monolayer with Gaussian diagonal disorder rather than topological disorder which corresponds to quantum percolation of excitons. Second, we represent numerical calculation for monolayers whose size is much larger than the optical wavelength. Third, we calculate and analyze the quantum yield for the coherent and the incoherent components. Finally, by going beyond the ladder approximation and including also the maximally crossed diagrams, we predict an additional backscattering peak in the signal. This peak is related to the exciton diffusion coefficient, which is calculated using the renormalization-group technique. Such a peak has been observed in three-dimensional samples in the off-resonance region,[19] where it is related to weak localization of light, and to similar effects such as phase conjugation,[20] long-time decay in transient grating,[21] etc. In this paper, we predict a backscattering peak in the luminescence, following a resonant excitation of a two-dimensional system, resulting from weak localization of excitons. The form of this peak reflects the size scaling of the diffusion coefficient. In two-dimensional systems, this size dependence is important for sufficiently large sizes even for very weak disorder.[22,23] The magnitude of the renormalization of the diffusion coefficient is limited by the exciton radiative decay, which restricts the range of parameters for observation of localization effects.

In Sec. II we introduce our model. In Sec. III we derive a Green-function expression for the fluorescence. In Sec. IV we calculate the coherent and the incoherent components of fluorescence. Finally in Sec. V we study the effects of exciton localization on the backscattering peak, and discuss the fundamental restrictions imposed by the radiative decay on observing exciton strong localization.

<u>50</u>   5609

II. MODEL AND HAMILTONIAN

Consider an infinite two-dimensional square lattice occupied by polarizable two-level molecules with nonoverlapping charge distributions. The total Hamiltonian in the Coulomb gauge and the multipolar form (neglecting magnetic terms) is[13,14]

$$\hat{H}_{\text{mult}} = \hat{H}_{\text{mat}} + \hat{H}_{\text{rad}} - \int d\mathbf{r}\, \hat{\mathbf{P}}(\mathbf{r}) \cdot \hat{\mathbf{D}}^{\perp}(\mathbf{r})$$
$$+ 2\pi \int d\mathbf{r} |\hat{\mathbf{P}}^{\perp}(\mathbf{r})|^2 . \tag{1}$$

We use a caret to denote operators, e.g., $\hat{O}$ and write $O(t)$ for its expectation value, and set $\hbar = 1$. $\hat{H}_{\text{mat}}$ is the material Hamiltonian,

$$\hat{H}_{\text{mat}} = \sum_m \Omega_m \hat{B}_m^+ \hat{B}_m + \sum_{m \neq n} J_{mn} \hat{B}_m^+ \hat{B}_n . \tag{2}$$

Here $\Omega_m = \Omega + U_m$ is the transition frequency of molecule at site m, where Ω is an average frequency and U_m is a random variable with a Gaussian statistics described by the correlation function

$$\overline{U_m U_n} = U_0^2 \delta_{mn} , \tag{3a}$$

$$\overline{U_m} = 0 . \tag{3b}$$

We denote configurational averaging with an overbar, and U_0 is the magnitude of the transition frequency fluctuations. J_{mn} is the dipole-dipole interaction, and $\hat{B}_m^+$ ($\hat{B}_m$) are creation (annihilation) operators of an exciton at site m, which satisfy the commutation relations

$$[\hat{B}_m, \hat{B}_n^+] = (1 - 2\hat{B}_m^+ \hat{B}_m) \delta_{mn} . \tag{4}$$

Note that $\hat{H}_{\text{mat}}$ conserves the number of excitons. This is the result of the Heitler-London approximation,[24] which holds for $\Omega \gg J_{mn}$. $\hat{H}_{\text{rad}}$ is the free radiation field Hamiltonian, and $\hat{D}^{\perp}(\mathbf{r})$ represents the transverse electric displacement. Both $\hat{H}_{\text{rad}}$ and $\hat{D}^{\perp}(\mathbf{r})$ are field operators which commute with all material operators. The transverse electromagnetic field $\hat{E}^{\perp}(\mathbf{r})$ is related to the electric displacement operator $\hat{D}^{\perp}(\mathbf{r})$ by

$$\hat{E}^{\perp}(\mathbf{r}) \equiv \hat{D}^{\perp}(\mathbf{r}) - 4\pi \hat{P}^{\perp}(\mathbf{r}) , \tag{5}$$

where $\hat{P}^{\perp}(\mathbf{r})$ is the transverse part of polarization. The polarization operator $\hat{P}(\mathbf{r})$ is

$$\hat{P}(\mathbf{r}) = \mu \sum_m \rho(\mathbf{r} - \mathbf{R}_m)(\hat{B}_m + \hat{B}_m^+) . \tag{6}$$

Here $\mathbf{R}_m$ is the position of the mth lattice point, and $\mu \rho(\mathbf{r} - \mathbf{R}_m)$ is the dipole density distribution of a molecule at site m, normalized as

$$\int d\mathbf{r} \rho(\mathbf{r} - \mathbf{R}_m) = 1 . \tag{7}$$

III. GREEN-FUNCTION EXPRESSION FOR FLUORESCENCE

We adopt the following convention for a temporal Fourier transform throughout this paper:

$$F(\omega) = \int_{-\infty}^{+\infty} dt\, e^{i\omega t} F(t) . \tag{8}$$

The linear susceptibility χ^{ext} with respect to external field $\mathbf{E}^{\text{ext}}$ is defined as

$$\mathbf{P}(\mathbf{r}, \omega) = \int d\mathbf{r}' \chi^{\text{ext}}(\mathbf{r}, \mathbf{r}', \omega) \cdot \mathbf{E}^{\text{ext}}(\mathbf{r}', \omega) . \tag{9}$$

Chernyak and Mukamel derived a Green-function expression for χ^{ext} for this model, using equations of motion in the Heisenberg picture.[14] In the rotating wave approximation, the result is

$$\chi^{\text{ext}}(\mathbf{r}, \mathbf{r}', \omega) = -\mu\mu \sum_{m,n} \rho(\mathbf{r} - \mathbf{R}_m) \rho(\mathbf{r}' - \mathbf{R}_n) G_{mn}(\omega) , \tag{10}$$

where the single-particle Green function G is defined as[16,17]

$$G_{mn}(\omega) = [\omega - H^{\text{eff}}(\omega) + i0]_{mn}^{-1} , \tag{11}$$

with the effective Hamiltonian matrix

$$H_{mn}^{\text{eff}}(\omega) = \Omega_m \delta_{mn} + J_{mn}$$
$$+ \int d\mathbf{r} \int d\mathbf{r}' \rho(\mathbf{r} - \mathbf{R}_m)$$
$$\times \rho(\mathbf{r}' - \mathbf{R}_n) \boldsymbol{\mu} \cdot \mathcal{G}^{\perp}(\mathbf{r} - \mathbf{r}', \omega) \boldsymbol{\mu} . \tag{12}$$

Note that $H^{\text{eff}}(\omega)$ is non-Hermitian. $\mathcal{G}$ is the vacuum Green function of the transverse electromagnetic field

$$\mathcal{G}^{\perp}(\mathbf{r}, \omega) = -\left[\left[\frac{\omega}{c}\right]^2 + \nabla\nabla\right] \frac{e^{i(\omega/c)r}}{r} + \nabla\nabla\frac{1}{r} , \tag{13a}$$

$$\mathcal{G}^{\perp}(\mathbf{q}, \omega) = \int d^3 r\, \mathcal{G}^{\perp}(\mathbf{r}, \omega) e^{-i\mathbf{q}\cdot\mathbf{r}}$$

$$= \frac{4\pi\omega^2}{\omega^2 - q^2 c^2 + i0} \left[1 - \frac{\mathbf{qq}}{q^2}\right] . \tag{13b}$$

The last term in Eq. (12) is the retarded correction to the dipole interaction. Its real part adds a radiative shift to the Coulomb interaction J_{mn}, and its imaginary part represents radiative decay. We make the Markovian approximation by replacing $H^{\text{eff}}(\omega)$ with $H^{\text{eff}}(\Omega)$. This is valid as long as the wave vector of the incident light is not nearly parallel to the plane.[17] The effective Hamiltonian can also be derived using projection operator techniques.[25,26] For $\Omega/c \ll 1/a$ (a being the lattice constant), the real part of the retardation correction is small, and we may keep only the imaginary part,

$$H_{mn}^{\text{eff}}(\omega) \to H_{mn}^{\text{eff}}(\Omega) = \Omega_m \delta_{mn} + J_{mn} - i\Gamma_{mn} . \tag{14}$$

We adopt the following convention of spatial Fourier transform for any function F_{mn} that depends only on $\mathbf{R}_m - \mathbf{R}_n$,

$$F(\mathbf{p}) = \sum_m F_{mn} \exp[-i\mathbf{p}\cdot(\mathbf{R}_m - \mathbf{R}_n)] . \tag{15}$$

Here $\mathbf{p}$ is a two-dimensional, in-plane vector, and the summation is over all lattice points. The spatial Fourier transform of Γ_{mn}, $\Gamma(\mathbf{p})$, is the total momentum-dependent decay rate

$$\Gamma(\mathbf{p}) \equiv \Gamma_r(\mathbf{p}) + \Gamma_{nr}(\mathbf{p}) , \tag{16}$$

where Γ_r and Γ_{nr} are the radiative and nonradiative decay rates. We assume that $\rho(\mathbf{r})$ is localized in space with size much smaller than the lattice constant; we can therefore use the point dipole approximation for intermolecular interactions, setting

$$\rho(\mathbf{r}) = \delta(\mathbf{r}) . \tag{17}$$

Keeping the lowest order in $\Omega a / c$, we have[16]

$$\Gamma_r(\mathbf{p}) = \frac{2\pi}{a^2} \frac{k_0^2 \mu^2 - (\mathbf{p} \cdot \mu^{\|})^2 - (k_0^2 - p^2)(\mu^{\perp})^2}{\sqrt{k_0^2 - p^2}} \Theta(k_0 - p) , \tag{18}$$

where $k_0 \equiv \Omega / c$ is the optical wave vector, and $\Theta(k_0 - p)$ is the Heaviside step function

$$\Theta(k_0 - p) = \begin{cases} 1 , & p < k_0 \\ 0 , & p > k_0 \end{cases} . \tag{19}$$

We denote the projection of a vector $\mathbf{A}$ parallel or normal to the lattice plane by $A^{\|}$ and $A^{\perp}$, respectively. Note that Γ_r satisfies the following sum rule:

$$\frac{1}{M} \sum_{\mathbf{p}} \Gamma_r(\mathbf{p}) \rightarrow \frac{a^2}{(2\pi)^2} \int d^2p \, \Gamma_r(\mathbf{p}) = \frac{\gamma_0}{2} , \tag{20}$$

with the single molecule radiative decay rate

$$\gamma_0 = 4\mu^2 k_0^3 / 3 . \tag{21}$$

The differential emission rate of radiation energy per solid angle, detected at position $\mathbf{R}$ far from the lattice, is

$$I(\hat{R}, t) = \frac{R^2 c}{2\pi} \overline{\langle E_{sc}^+(\mathbf{R}, t) E_{sc}(\mathbf{R}, t) \rangle}$$

$$\simeq \frac{R^2 c}{2\pi} \overline{|\langle E_{sc}(\mathbf{R}, t) \rangle|^2} , \tag{22}$$

where $\hat{R} = \mathbf{R}/R$, and E_{sc} denotes the scattered field. We use $\langle \ \rangle$ to denote the quantum-mechanical expectation value for a given realization of the disorder, and an overbar to denote the average over disorder. In Eq. (22), we have factorized the quantum-mechanical average and thus neglected quantum fluctuations of the field. In the far zone where $R \gg \lambda$ ($\lambda \equiv 2\pi/k_0$ is the optical wavelength), the field is purely transverse and we have

$$\mathbf{E}_{sc}(\mathbf{R}, t) = -\int \frac{d\omega}{2\pi} \int d\mathbf{r} \, \mathscr{G}^{\perp}(\mathbf{R} - \mathbf{r}, \omega) \cdot \mathbf{P}(\mathbf{r}, \omega)$$

$$\times \exp(-i\omega t) . \tag{23}$$

For R much larger than the optical wavelength λ and the lattice size, we have from Eq. (13a)

$$\mathscr{G}^{\perp}(\mathbf{R} - \mathbf{r}, \omega) \simeq -k_0^2 (1 - \hat{R}\hat{R}) e^{ik_0 R} e^{-ik_0 \hat{R} \cdot \mathbf{r}} / R . \tag{24}$$

The external field is taken to be of the form

$$\mathbf{E}^{ext}(\mathbf{r}, \omega) = E(\omega) \exp(i\boldsymbol{\kappa} \cdot \mathbf{r}) \mathbf{e}_1 , \tag{25}$$

with $\kappa = \Omega / c$ and $\mathbf{e}_1$ being the unit vector of the polarization direction of the field ($\mathbf{e}_1 \perp \hat{\kappa}$).

Substituting Eq. (25) into Eq. (9) and then into Eqs. (23) and (22), and using Eq. (24), we get

$$I(\hat{R}, t) = A \int \int d\omega_1 d\omega_2 \phi(\mathbf{k}', \mathbf{k}, \mathbf{q} = 0; \omega_1, \omega_2)$$

$$\times E(\omega_1) E^*(\omega_2) \exp(-i\omega_{12} t) . \tag{26}$$

We have set $t - R/c \rightarrow t$ and use the point dipole approximation Eq. (17). Here

$$A \equiv \frac{M\Omega^4 (\mu \cdot \mathbf{e}_1)^2 (\mu \cdot \mathbf{e}_2)^2}{8\pi^3 c^3} , \tag{27}$$

M is the number of molecules, $\mathbf{k}$ and $\mathbf{k}'$ are the in-plane projection of κ and $k_0 \hat{R}$, $\mathbf{e}_2$ is the unit vector of the polarization direction of E_{sc} with $\mathbf{e}_2 \perp \hat{R}$, and $\omega_{12} \equiv \omega_1 - \omega_2$.

The particle-hole Green function ϕ is defined as

$$\phi(\mathbf{k}', \mathbf{k}, \mathbf{q}; \omega_1, \omega_2) \equiv \frac{1}{M} \sum_{m_1, m_2, m_3, m_4} \overline{G_{m_1 m_2}(\omega_1) G^*_{m_3 m_4}(\omega_2)}$$

$$\times \exp[-i(\mathbf{k}' + \mathbf{q}/2)\mathbf{R}_{m_1} + i(\mathbf{k} + \mathbf{q}/2) \cdot \mathbf{R}_{m_2} + i(\mathbf{k}' - \mathbf{q}/2) \cdot \mathbf{R}_{m_3} - i(\mathbf{k} - \mathbf{q}/2) \cdot \mathbf{R}_{m_4}] . \tag{2}$$

Equation (26) coincides with the result of Wang, Muenter, and Mukamel[18] which was obtained by calculating the photon emission rate using a quantum description of the radiation field. Here the radiation field is treated classically and the fluorescence signal is obtained by solving the Maxwell equations [see Eq. (23)].

IV. COHERENT AND INCOHERENT COMPONENTS OF FLUORESCENCE

In the preceding section, we expressed the fluorescence signal formally in terms of a p-h Green function [see Eq. (26)] ϕ, which is the disorder averaged product of two single-particle Green functions [see Eq. (28)]. In this section, we will evaluate ϕ in the weak disorder limit

$$f_0 \equiv \frac{8a^2}{\pi D(\omega_0, \omega_0) \rho(\omega_0)} \ll 1 , \tag{29}$$

where ω_0 is the excitation frequency, $\rho(\omega_0)$ is the density of single exciton states

$$\rho(\omega_0) = -\frac{1}{\pi} \text{Im} \overline{G}_{nn}(\omega_0) , \tag{30}$$

and $D(\omega_0, \omega_0)$ is the exciton diffusion coefficient defined later. In this case, the p-h Green function $\phi(\mathbf{k}', \mathbf{k}, \mathbf{q}; \omega_1, \omega_2)$ (and the fluorescence signal) is given by a sum of three terms

$$\phi = \phi_c + \phi_I + \phi_{bs} , \tag{31}$$

$$I(\hat{R}, t) = A[S_c(t) + S_I(t) + S_{bs}(t)] . \tag{32}$$

S_c, S_I, and S_{bs} denote the coherent, the incoherent, and the backscattering components, obtained by substituting ϕ_c, ϕ_I, and ϕ_{bs} into Eq. (26), respectively.

In the absence of disorder, ϕ_I and ϕ_{bs} vanish, and the signal consists of the coherent component alone. ϕ_c is simply a product of two averaged Green functions

$$\phi_c(\mathbf{k}',\mathbf{k},\mathbf{q};\omega_1,\omega_2)=G(\mathbf{k}'+\mathbf{q}/2,\omega_1)G^*(\mathbf{k}-\mathbf{q}/2,\omega_2)$$
$$\times(2\pi/a)^2\delta(\mathbf{k}'-\mathbf{k}) , \quad (33)$$

and the coherent signal, which is strongly peaked in the forward direction $\mathbf{k}'=\mathbf{k}$, is given by

$$S_c(t)=\left|\frac{2\pi}{a}\right|^2\left|\int d\omega\, G(\mathbf{k},\omega)E(\omega)e^{-i\omega t}\right|^2\delta(\mathbf{k}-\mathbf{k}') .$$
$$(34)$$

This signal represents the transmitted and the reflected waves. In Eq. (34), $G(\mathbf{k},\omega)$ is the disorder-averaged single-particle Green function in momentum space. We assume

$$G(\mathbf{k},\omega)=\frac{1}{\omega-\epsilon(\mathbf{k})-\Sigma(\omega)+i\Gamma(\mathbf{k})} , \quad (35)$$

with $\epsilon(\mathbf{k})$ being the exciton energies:

$$\epsilon(\mathbf{k})\equiv\Omega+J(\mathbf{k}) . \quad (36)$$

The self-energy $\Sigma(\omega)$ will be determined by the following self-consistent equation:[22,27]

$$\Sigma(\omega_0)=\frac{U_0^2 a^2}{4\pi^2}\int d\mathbf{k}\, G(\mathbf{k},\omega_0) , \quad (37)$$

which holds for weak disorder. The single exciton density of states is related to the imaginary part of the Green function,

$$\rho(\omega)=-\frac{a^2}{4\pi^3}\int d\mathbf{p}\,\mathrm{Im}G(\mathbf{p},\omega)=-\frac{1}{\pi U_0^2}\mathrm{Im}\Sigma(\omega) . \quad (38)$$

Under impulsive excitation, $E(t)=\delta(t)$, $S_c(t)$ decays exponentially with the rate $-\mathrm{Im}\Sigma_k+\Gamma(\mathbf{k})$, where $\Sigma_k\equiv\Sigma[\omega=\epsilon(\mathbf{k})]$. Note that $\mathrm{Im}\Sigma(\omega)$ is negative, and $-\mathrm{Im}\Sigma_k$ is the scattering rate of excitons with momentum $\mathbf{k}$ by impurities. Once scattered, the exciton no longer contributes to the forward coherent signal. $\Gamma(\mathbf{k})$ is the superradiant decay rate of a regular lattice ($U_0=0$). For normal incidence, i.e., $\mathbf{k}=0$, we have

$$\Gamma(0)=\frac{3}{8\pi}\gamma_0(\lambda/a)^2(\mu^\parallel/\mu)^2 , \quad (39)$$

where $\lambda\equiv2\pi/k_0$ is the optical wavelength. This is enhanced by a factor of $(\lambda/a)^2$ compared with the single molecule decay rate γ_0.

ϕ_I contributes an incoherent component S_I to the fluorescence signal, which shows up as a homogeneous background in its angular dependence. In the ladder approximation, we have[23,28]

$$\phi_I(\mathbf{k}',\mathbf{k},\mathbf{q};\omega_1,\omega_2)=G(\mathbf{k}'+\mathbf{q}/2,\omega_1)$$
$$\times G(\mathbf{k}+\mathbf{q}/2,\omega_1)G^*(\mathbf{k}'-\mathbf{q}/2,\omega_2)$$
$$\times G^*(\mathbf{k}-\mathbf{q}/2,\omega_2)\mathcal{D}(\mathbf{q};\omega_1,\omega_2) \quad (40)$$

and

$$S_I(t)=\int d\omega_1\int d\omega_2 G(\mathbf{k}',\omega_1)G^*(\mathbf{k}',\omega_2)G(\mathbf{k},\omega_1)$$
$$\times G^*(\mathbf{k},\omega_2)\mathcal{D}(0;\omega_1,\omega_2)E(\omega_1)$$
$$\times E^*(\omega_2)e^{-i\omega_{12}t} . \quad (41)$$

In Eq. (40) $\mathcal{D}$ is the diffusion propagator[22] which has the following form in the ladder approximation:

$$\mathcal{D}(\mathbf{q};\omega_1,\omega_2)=\frac{U_0^2}{1-U_0^2 L(\mathbf{q};\omega_1,\omega_2)} , \quad (42)$$

with

$$L(\mathbf{q};\omega_1,\omega_2)=\frac{a^2}{4\pi^2}\int d\mathbf{p}\, G(\mathbf{p}+\mathbf{q}/2,\omega_1)G^*(\mathbf{p}-\mathbf{q}/2,\omega_2) .$$
$$(43)$$

In the small-q limit, we have (see Appendix A)

$$\mathcal{D}(\mathbf{q};\omega_1,\omega_2)=\frac{U_0^2[\omega_{12}-\Sigma(\omega_1)+\Sigma^*(\omega_2)+i\gamma(\omega_1,\omega_2)]}{\omega_{12}+i\gamma(\omega_1,\omega_2)+iq^2 D(\omega_1,\omega_2)} ,$$
$$(44)$$

where $D(\omega_1,\omega_2)$ is the bare exciton diffusion coefficient,

$$D(\omega_1,\omega_2)=\frac{i}{4}U_0^2[-\omega_{12}+\Sigma(\omega_1)-\Sigma^*(\omega_2)-i\gamma(\omega_1,\omega_2)]$$
$$\times\left|\frac{a}{2\pi}\right|^2\int d\mathbf{p}|\mathbf{v}(\mathbf{p})|^2 G^2(\mathbf{p},\omega_1)G^{*2}(\mathbf{p},\omega_2) ,$$
$$(45)$$

with the exciton velocity $\mathbf{v}(\mathbf{p})=\nabla_\mathbf{p}J(\mathbf{p})-i\nabla_\mathbf{p}\Gamma(\mathbf{p})$, and

$$\gamma(\omega_1,\omega_2)=\frac{2\int d\mathbf{p}\,\Gamma(\mathbf{p})G(\mathbf{p},\omega_1)G^*(\mathbf{p},\omega_2)}{\int d\mathbf{p}\, G(\mathbf{p},\omega_1)G^*(\mathbf{p},\omega_2)} . \quad (46)$$

The bare exciton diffusion coefficient for a topologically disordered system is calculated previously.[29] Since the incoherent component S_I is related to $\mathcal{D}(\mathbf{q},\omega_1,\omega_2)$ with $q=0$ [see Eq. (41)], the diffusion coefficient D in Eq. (44) does not affect S_I.

We next define

$$\omega_0\equiv\frac{\omega_1+\omega_2}{2} , \quad \omega_{12}\equiv\omega_1-\omega_2 . \quad (47)$$

When the total population decay rate $\gamma(\omega_0,\omega_0)$ is much smaller than the inhomogeneous broadening $|\mathrm{Im}\Sigma(\omega_0)|$ and the spectral width of excitation pulse, the long-time behavior of $S_I(t)$ [Eq. (41)] is determined by the poles at $\omega_{12}=-i\gamma(\omega_1,\omega_2)$,

$$S_I(t)=-4\pi U_0^2\int d\omega_0|G(\mathbf{k}',\omega_0)|^2|G(\mathbf{k},\omega_0)|^2$$
$$\times\mathrm{Im}\Sigma(\omega_0)|E(\omega_0)|^2 e^{-\gamma(\omega_0)t} , \quad (48)$$

where

$$\gamma(\omega_0) \equiv \gamma(\omega_0, \omega_0) \equiv \frac{2\sum_{\mathbf{p}} \Gamma(\mathbf{p})|G(\mathbf{p}, \omega_0)|^2}{\sum_{\mathbf{p}} |G(\mathbf{p}, \omega_0)|^2} ,$$ (49)

is the energy-dependent exciton decay rate.[18]

Our model does not allow for relaxation among the various exciton states in the band, and thus the energy-dependent decay rate can be measured experimentally by applying a pulse with linewidth much narrower than the inhomogeneous dephasing rate $-\mathrm{Im}\Sigma(\omega_0)$ and much larger than the total population decay rate $\gamma(\omega_0)$. Then the incoherent signal decays exponentially $S_I(t) \sim e^{-\gamma(\omega_0)t}$, with ω_0 being the excitation frequency. By tuning ω_0, one can measure the energy-dependent exciton decay rate $\gamma(\omega_0)$. In practice, neglecting relaxation among the exciton states is justified only for very low temperatures and relatively short times. As relaxation takes place, emission will be dominated by the lowest states in the band, and the frequency dependence of $\gamma(\omega_0)$ may not be readily observable.

We next calculate the total emitted energy

$$\int d\hat{R} \sum_{\mathbf{e}_2} \int dt\, I(t) ,$$

where $\int d\hat{R}$ denotes integrating over the solid angle, and $\sum_{\mathbf{e}_2}$ implies summation over the two possible polarizations of the scattered field. In Appendix B, we prove the following sum rules:

$$\int d\hat{R} \sum_{\mathbf{e}_2} (\mathbf{e}_2 \cdot \boldsymbol{\mu})^2 \int dt\, S_c(t)$$

$$= \frac{8\pi^2}{\mu^2 k_0^3} \int d\omega_0 Y_c(\omega_0) \mathrm{Im}\chi^{\mathrm{ext}}(\mathbf{k}, \omega_0)|E(\omega_0)|^2$$ (50)

and

$$\int d\hat{R} \sum_{\mathbf{e}_2} (\mathbf{e}_2 \cdot \boldsymbol{\mu})^2 \int dt\, S_I(t)$$

$$= \frac{8\pi^2}{\mu^2 k_0^3} \int d\omega_0 Y_I(\omega_0) \mathrm{Im}\chi^{\mathrm{ext}}(\mathbf{k}, \omega_0)|E(\omega_0)|^2 ,$$ (51)

where

$$Y_c(\omega_0) = \frac{\Gamma_r(\mathbf{k})}{-\mathrm{Im}\Sigma(\omega_0) + \Gamma(\mathbf{k})}$$ (52)

is the quantum yield for the coherent signal,

$$Y_I = \frac{-\mathrm{Im}\Sigma(\omega_0)}{-\mathrm{Im}\Sigma(\omega_0) + \Gamma(\mathbf{k})} \frac{\gamma_r(\omega_0)}{\gamma(\omega_0)}$$ (53)

is the quantum yield for the incoherent signal,

$$\mathrm{Im}\chi^{\mathrm{ext}}(\mathbf{k}, \omega_0) = \mu^2[-\mathrm{Im}\Sigma(\omega_0) + \Gamma(\mathbf{k})]|G(\mathbf{k}, \omega_0)|^2$$ (54)

is the linear absorption coefficient, and $\gamma_r(\omega_0)$ is the energy-dependent radiative decay rate

$$\gamma_r(\omega_0) \equiv \frac{2\sum_{\mathbf{p}} \Gamma_r(\mathbf{p})|G(\mathbf{p}, \omega_0)|^2}{\sum_{\mathbf{p}} |G(\mathbf{p}, \omega_0)|^2} .$$ (55)

The total incoherent signal given by Eq. (51) is an observable, while the total coherent signal given by Eq. (50) is not, since the coherent signal in the transmitted direction mixes with the incident field. However, the total reflected signal is an observable given by (see Appendix B)

$$\int_{\mathrm{ref}} d\hat{R} \sum_{\mathbf{e}_2} (\mathbf{e}_2 \cdot \boldsymbol{\mu})^2 \int dt\, S_c(t)$$

$$= \frac{8\pi^2}{\mu^2 k_0^3} \int d\omega_0 Y_r(\omega_0) \mathrm{Im}\chi^{\mathrm{ext}}(\mathbf{k}, \omega_0)|E(\omega_0)|^2 ,$$ (56)

where $\int_{\mathrm{ref}} d\hat{R}$ denotes integration over the solid angle in the vicinity of the reflected direction $\hat{R} = \hat{\kappa}_r \equiv \hat{\kappa}^{\parallel} - \hat{\kappa}_z \hat{z}$, and Y_r is the reflection yield

$$Y_r(\omega_0) = \frac{\mu^2 - (\boldsymbol{\mu} \cdot \hat{\kappa}_r)^2}{2\mu^2 - (\boldsymbol{\mu} \cdot \hat{\kappa})^2 - (\boldsymbol{\mu} \cdot \hat{\kappa}_r)^2} Y_c(\omega_0) .$$ (57)

If $\boldsymbol{\mu}$ is in-plane, $Y_r = Y_c/2$, i.e., half of the coherent signal is reflected (transmitted).

The temporal profile of the spontaneous emission can be interpreted using the following simple picture: Excitation with a short resonant pulse creates excitons with momentum $\mathbf{k}$ equal to the projection of the incident wave vector onto the lattice plane. Subsequent evolution of these excitons is caused by three mechanisms: the exciton can either decay radiatively with rate $2\Gamma_r(\mathbf{k})$ (coherent radiative decay with photon emitted in the forward direction), decay nonradiatively with rate $2\Gamma_{\mathrm{nr}}(\mathbf{k})$, or be scattered with scattering rate $-2\,\mathrm{Im}\Sigma(\omega_0)$. The coherent component is generated when a photon is emitted prior to the first scattering even; the exciton momentum is conserved and the signal is emitted in the forward direction. The incoherent component results from emission after at least one scattering event. When the excitation frequency ω_0 is not too close to the band edge, the exciton becomes nonradiative after scattering. To emit a photon, the exciton needs to be scattered back to the radiative region. The low probability of this process due to the small relative volume of the radiative region, leads to the long emission time scale of the incoherent component. Since the momentum of the final exciton state $\mathbf{k}'$ prior to emission is confined in a small region $k' < k_0$, the last scattering process is virtually independent on $\mathbf{k}'$. This leads to the homogeneous angular distribution of the incoherent component.

The temporal profile of the coherent component depends on the radiative and scattering rates. A radiative exciton created by the excitation pulse can leave the radiative region in two ways: it can either emit a photon or scatter to the nonradiative region. The first process is irreversible and contributes to the coherent component. In the second case, the exciton goes through a long and random walk of multiple scattering events, before it returns to the radiative region, where it emits a photon and con-

tributes to the incoherent component. According to this picture, if the radiative decay rate (the super-radiant rate of radiative excitons) is much larger than the scattering rate, the coherent component time scale will be dominated by the super-radiant lifetime, and almost all photons will be emitted in the coherent channel so that the quantum yield Y_c [Eq. (52)] approaches unity (assuming no nonradiative damping). In the opposite limit, the coherent component time scale is determined by the scattering time, and most photons are emitted in the incoherent channel, setting Y_I to unity. Note that in the absence of nonradiative damping [$\Gamma_{nr}(\mathbf{k})=0)$], $\gamma(\omega_0)=\gamma_r(\omega_0)$, and $Y_I+Y_c=1$. For a regular lattice ($U_0=0$), $Y_I(\omega_0)=0$, and the homogeneous background scattering vanishes.

As will be shown in the next section, the backscattering signal S_{bs} is peaked in the backward direction and its peak intensity has the same magnitude as the incoherent signal. Therefore the backscattering quantum yield is negligible compared with the incoherent signal, and it may be safely neglected in the above expressions.

We have calculated the time-resolved spontaneous emission of a molecular monolayer with Gaussian diagonal disorder whose physical dimensions are much larger than the optical wavelength and the exciton mean free path. In the following numerical calculations we modeled the aggregate as a square lattice with unit cell vectors $a\hat{x}$ and $a\hat{y}$. The transition dipole μ is taken to be in-plane,

$$\mu = \frac{\mu}{\sqrt{2}}(\hat{x}+\hat{y}) \ .$$

We further assume nearest-neighbor interactions, so that

$$J(\mathbf{p}) = -W[\cos(p_x a)+\cos(p_y a)] \ , \tag{58}$$

$4W$ is the bandwidth of a regular lattice ($U_0=0$), with $W=\mu^2/a^3$. For the present geometry, the nearest-neighbor interaction is negative (J aggregate). $\lambda\equiv 2\pi/k_0=10^3 a$. The momentum-dependent decay rate is $\Gamma(\mathbf{k})=\Gamma_r(\mathbf{k})+\eta$, with $\Gamma_r(\mathbf{k})$ given by Eq. (18) and $\eta=10^{-6}W$ is a constant. 2η represents a nonradiative decay rate.

The energy-dependent inhomogeneous dephasing rate $\tau^{-1}\equiv -2\,\mathrm{Im}\Sigma(\omega_0)$ as a function of ω_0, obtained by solving Eq. (37) for various values of U_0, is displayed in Fig. 1. From bottom to top, $U_0/W=0.01,0.02,0.03$. τ^{-1} increase with the degree of disorder U_0. Equation (37) shows that in the weak disorder limit, $\Sigma\sim U_0^2$. As can be seen from Eq. (38), the frequency profile of $[\tau(\omega_0)]^{-1}$ is identical to the density of states. The density of states of a regular two-dimensional lattice with nearest-neighbor interaction has a logarithmic singularity at the band center,[30,31] and the peak at the band center in Fig. 1 reflects this singularity. Our theory holds only when

$$[\gamma(\omega_0)\tau(\omega_0)]^{-1}\gg 1 \tag{59}$$

and

$$f_0^{-1}\equiv \frac{\pi D(\omega,\omega)\rho(\omega)}{8a^2}\gg 1 \ . \tag{60}$$
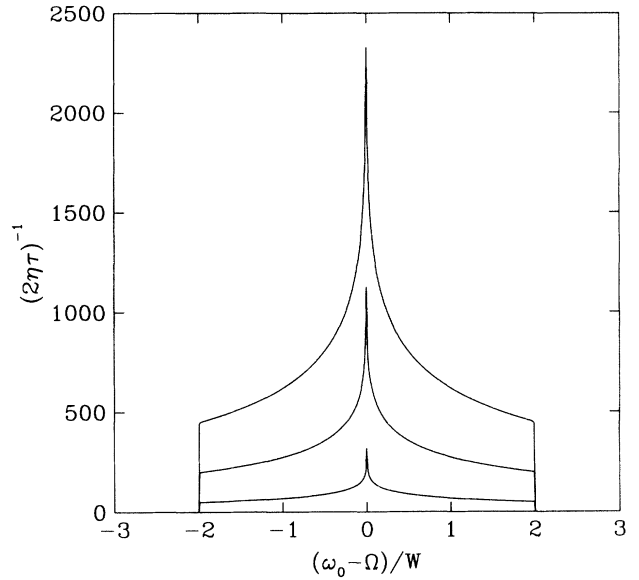
FIG. 1. Disorder-induced dephasing rate $[\tau(\omega_0)]^{-1}$ divided by the nonradiative decay rate 2η as a function of exciton energy ω_0. $\eta=10^{-6}W$. From bottom to top, $U_0/W=0.01,0.02,0.03$.

For the parameters used in our numerical calculation, the nonradiative decay rate is much larger than the radiative decay rate, and $\gamma(\omega_0)\simeq 2\eta=2\times 10^{-6}W$. $(2\eta\tau)^{-1}$ and f_0^{-1} as a function of ω_0 are displayed in Figs. 1 and 2, respectively. The figures show that both conditions Eqs. (59) and (60) are satisfied provided ω_0 is not too close to the band edge.

The frequency-dependent radiative decay rate $\gamma_r(\omega_0)$ (in units of the single molecular radiative decay rate γ_0) is shown in Fig. 3. From left to right, $U_0/W=0.01,0.02,0.03$. We stay away from the band edge to
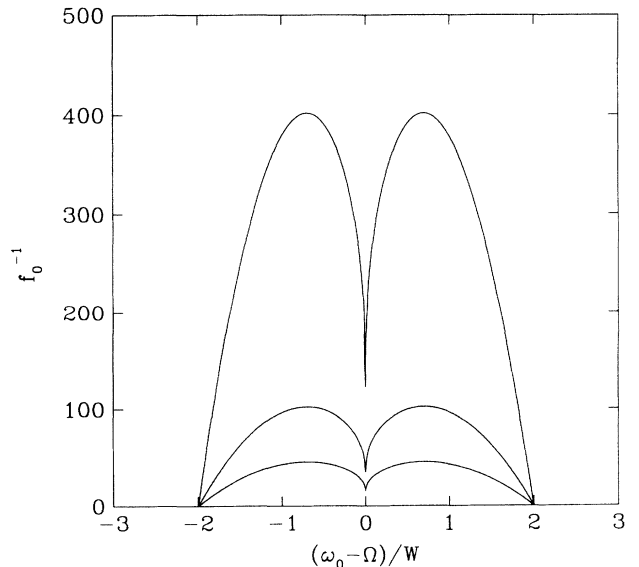
FIG. 2. f_0^{-1} as a function of exciton energy ω_0. $\eta=10^{-6}W$. From top to bottom, $U_0/W=0.01,0.02,0.03$.
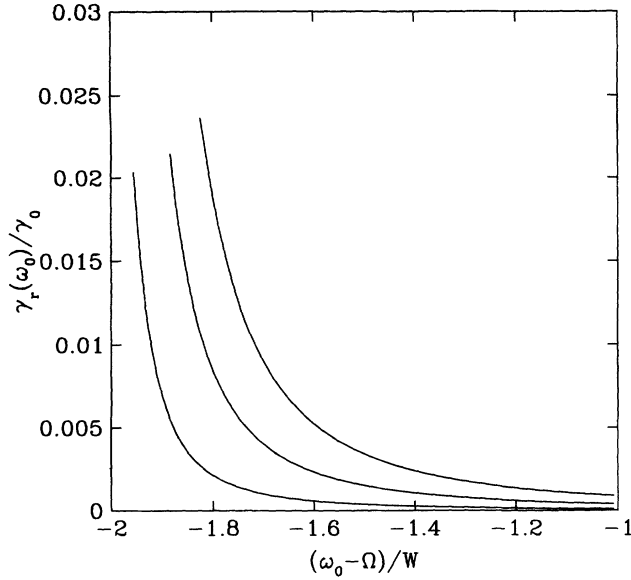
FIG. 3. Exciton radiative decay rate $\gamma_r(\omega_0)$ (normalized to the single molecular radiative decay rate γ_0) as a function of energy ω_0. $\eta = 10^{-6}W$. From the left to the right, $U_0/W = 0.01, 0.02, 0.03$.

keep $[\gamma(\omega_0)\tau(\omega_0)]^{-1} \geq 10$ and $f_0^{-1} \geq 10$. In this frequency region, the excitation pulse creates an exciton with momentum $k > k_0$, which is nonradiative [see Eq. (18)]. However, due to disorder, the exciton has finite probability to be scattered back to the radiative region $(k < k_0)$. The exciton radiative decay rate is therefore finite but very small (even smaller than the single molecular radiative decay rate γ_0), since the radiative region occupies only a very small part of the Brillouin zone, and the probability of the exciton to be scattered to the radiative region is low. $\gamma(\omega_0)$ increases with disorder since exciton scattering is enhanced.

V. BACKSCATTERING PEAK AND WEAK LOCALIZATION OF EXCITONS

We next consider ϕ_{bs} in Eq. (31), which is given by the sum of maximally crossed diagrams

$$\phi_{bs}(k',k,q;\omega_1,\omega_2) = G(k'+q/2,\omega_1)G(k+q/2,\omega_1)$$
$$\times G^*(k'-q/2,\omega_2)G^*(k-q/2,\omega_2)$$
$$\times \mathcal{D}(k'+k;\omega_1,\omega_2) . \tag{61}$$

In the ladder diagram approximation, $\mathcal{D}$ is given by Eq. (44). Therefore its contribution to the fluorescence signal S_{bs} is peaked in the direction opposite to the incident light $(k' = -k)$,

$$S_{bs}(t) = \int d\omega_1 \int d\omega_2 G(k',\omega_1)G^*(k',\omega_2)G(k,\omega_1)$$
$$\times G^*(k,\omega_2)\mathcal{D}(k+k';\omega_1,\omega_2)E(\omega_1)$$
$$\times E^*(\omega_2)e^{-i\omega_{12}t} . \tag{62}$$

The backscattering signal carriers information on the exciton diffusion coefficient D.

It is well known that in two dimensions the diffusion approximation breaks down for sufficiently large distances (or equivalently for small wave vectors) even for weak disorder.[22] This leads to the strong decrease of the diffusion constant D with decreasing wave vector, which should show up in the angular profile of the backscattering peak. Formally, the behavior of the Green function for small wave vectors can be described by considering the interaction of excitons with diffusion modes, whose dynamics are described by a nonlinear supersymmetric sigma model.[22] Then Eqs. (61) and (62) still hold if we treat the diffusion propagator $\mathcal{D}$ as a correlation function in the sigma model. The ladder approximation then corresponds to a complete neglect of the nonlinear interaction in the sigma model, i.e., the interaction of diffusion modes. Assuming $\gamma(\omega_0,\omega_0)\tau \ll 1$, and using the renormalization-group technique for the sigma model, we can evaluate the infrared asymptotics (small ω_{12}) of the diffusion propagator and obtain (for derivation see Appendix C)

$$\mathcal{D}(q,\omega_1,\omega_2) = \frac{U_0^2[\tau(\omega_0)]^{-1}}{-i\omega_{12}+\gamma(\omega_0)+q^2 D_r(q,\omega_1,\omega_2)} , \tag{63}$$

where D_r is the renormalized diffusion coefficient. For small q and ω_{12},

$$D_r(q,\omega_1,\omega_2) = D(\omega_0,\omega_0)\left[1 - \frac{a^2}{4\pi^2 D(\omega_0,\omega_0)\rho(\omega_0)}\ln\left[\frac{1}{[-i\omega_{12}+\gamma(\omega_0)]\tau(\omega_0)}\right]\right] , \tag{64}$$

and we have used the notation of Eq. (47).

For a continuous-wave incoming field with frequency ω_0, i.e., $E(\omega_0) = E_0\delta(\omega-\omega_0)$, the signal in the vicinity of the backscattering direction $(k' \simeq -k)$ is

$$S_I + S_{bs} = |G(k,\omega_0)|^2|G(-k,\omega_0)|^2|E_0|^2 U_0^2[\tau(\omega_0)]^{-1}\left[\frac{1}{\gamma(\omega_0)} + \frac{1}{\gamma(\omega_0)+|k+k'|^2 D_r(\omega_1,\omega_2)}\right] , \tag{65}$$

with k' being the projection of signal wave vector $k_0\hat{R}$ on the lattice plane. Equation (65) shows that the signal at the exact backscattering direction $k' = -k$ is twice the background signal. Since in the present approximation, the renormalized diffusion coefficient does not depend on $q = k + k'$ [see Eq. (64) and Appendix C], we use the abbreviated notation $D_r(\omega_1,\omega_2) \equiv D_r(q,\omega_1,\omega_2)$ in Eq. (65) and hereafter.

In a time domain experiment, when the total population decay rate $\gamma(\omega_0)$ is much smaller than the inhomogeneous

broadening $2|\mathrm{Im}\Sigma(\omega_0)|$ and the spectral width of excitation pulse, the total signal near the backscattering direction is

$$S_I(t)+S_{\mathrm{bs}}(t)=2\pi U_0^2 \int d\omega_0 |G(\mathbf{k},\omega_0)|^2 |G(-\mathbf{k},\omega_0)|^2 [\tau(\omega_0)]^{-1}|E(\omega_0)|^2 e^{-\gamma(\omega_0)t}[1+e^{-(\mathbf{k}+\mathbf{k}')^2 D_r(\omega_0,\omega_0)t}] \ . \qquad (66)$$

Assuming that the excitation pulse linewidth is much smaller than the exciton bandwidth [but still much larger than the decay rate $\gamma(\omega_0)$], the time- and angular-dependent signal near the backscattering direction is

$$S_I(t)+S_{\mathrm{bs}}(t)\sim e^{-\gamma(\omega_0)t}[1+e^{-(\mathbf{k}+\mathbf{k}')^2 D_r(\omega_0,\omega_0)t}] \ , \qquad (67)$$

where ω_0 is the central frequency of excitation pulse. The signal is peaked in direction $\mathbf{k}'=-\mathbf{k}$, and the spatial width of the peak $\delta k'$ is determined by $\delta k'^2=[D_r(\omega_0,\omega_0)t]^{-1}$. As time increases, $\delta k'$ decreases and the backscattering peak becomes sharper.

The energy-dependent bare diffusion coefficient $D(\omega_0,\omega_0)$ is displayed in Fig. 4. From top to bottom, $U_0/W=0.01,0.02,0.03$. D decreases as the disorder increases. The dip at $\omega_0=0$ reflects the maximum of the inhomogeneous dephasing rate τ^{-1} at $\omega_0=0$ (see Fig. 1). D has then a minimum, since the exciton is more effectively scattered.

D_r/D as a function of exciton energy ω_0 at various values of U_0 and η are displayed in Fig. 5. The figure shows that D_r/D decrease with increasing disorder or decreasing nonradiative damping η. It is believed that in two-dimensional systems, all states are localized.[23] However, excitons have a finite lifetime $\tau_d=1/[2\eta+\gamma(\omega)]$. Localization effects are negligible if $v\tau_d$ is much smaller than the localization length (v is the velocity of exciton). When $v\tau$ is comparable to the localization length, the localization effect is important and D_r becomes smaller than D. As η decreases, the exciton lifetime increases. As the disorder increases, the exciton localization length decreases. This leads to the reduction of D_r/D as η decreases and U_0 increases. Figure 5 shows that D_r/D is
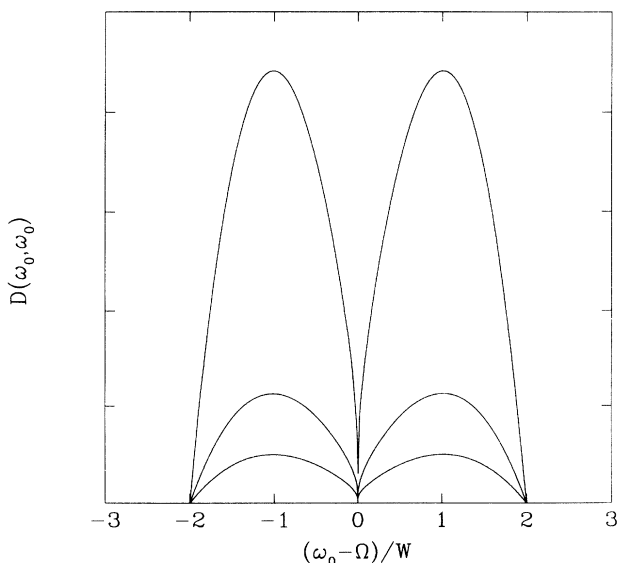
smallest in the vicinity of the band edge where the localization length is the smallest. However, it is still very close to unity.

The backscattering peak is usually attributed to weak localization of light and is described by the maximally crossed diagrams,[19] which go beyond the ladder diagram approximation, (i.e., regular diffusion). However, due to time-reversal symmetry,[23,28] the sum of the maximally crossed diagrams can be expressed in terms of a sum of ladder diagrams, which are related to diffusion properties (we can denote it diffusion in the cooperon channel), i.e, the bare diffusion coefficient $D(\omega_0,\omega_0)$. Here, we went beyond the diffusion approximation in the cooperon channel and looked for the scaling dependence of the diffusion coefficient. This scaling shows up in the backscattering form in the following way: The intensity in the direction forming the angle θ with the exact backscattering direction is determined by excitons which experienced diffusion on the length scale $L \sim \lambda/\theta$, λ being the optical wavelength. Therefore the dependence of the diffusion coefficient on L can show up in the angular profile of the peak. Note that the form of the backscattering peak from a two-dimensional structure differs from that from a semi-infinite medium even if we neglect the decrease of the diffusion coefficient with size. However, the size scaling of the diffusion coefficient is an effect of strong localization since it shows up when the length L approaches the localization scale.

Finally we discuss some limitations imposed by radiative decay on observing strong exciton localization in two-dimensional molecular aggregates. It is believed that in two dimensions, all states are localized even for

FIG. 4. Bare diffusion coefficient $D(\omega_0,\omega_0)$ as a function of energy ω_0. $\eta=10^{-6}W$. From top to bottom, $U_0/W = 0.01,0.02,0.03$.
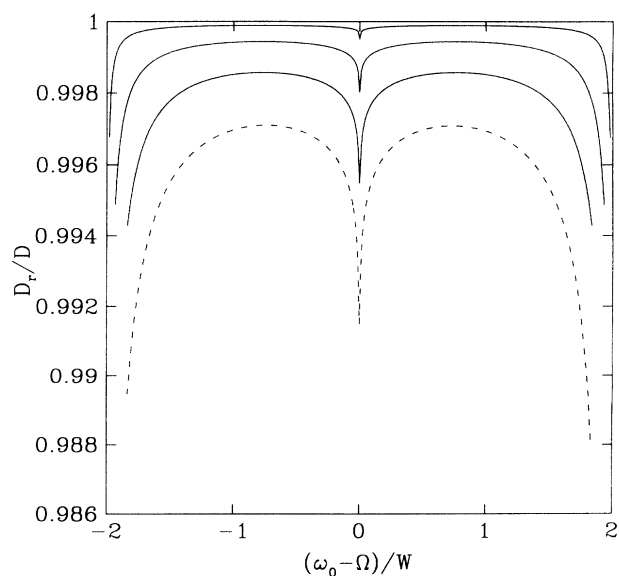
FIG. 5. Renormalized diffusion coefficient D_r (normalized to the bare diffusion coefficient D) as a function exciton energy ω_0. Solid lines $\eta=10^{-6}W$, from top to bottom, $U_0/W =0.01,0.02,0.03$. Dashed line $\eta=10^{-9}W$, and $U_0/W=0.03$.

infinitely weak disorder.[23] However with finite exciton lifetime, localization effects can only be observed provided the localization length is shorter than the mean free path associated with damping. A criterion can be easily obtained from Eq. (C7). Since localization implies vanishing of the renormalized diffusion coefficient f^{-1}, and the modulus of the logarithm in the right-hand side (rhs) of Eq. (C7) cannot be larger than $\ln[1/\gamma(\omega_0)\tau(\omega_0)]$, this criterion implies

$$f_0^{-1} \equiv \frac{\pi\rho(\omega_0)D(\omega_0,\omega_0)}{8a^2} \leq \frac{1}{32\pi}\ln\left[\frac{1}{\gamma(\omega_0)\tau(\omega_0)}\right] . \quad (68)$$

Since radiative decay is always present in a two-dimensional exciton system, we will apply Eq. (68) for radiative damping, i.e., replacing $\gamma(\omega_0)$ by $\gamma_r(\omega_0)$. If ω_0 is not too close to the band edge, we can set

$$G(\mathbf{p},\omega_0) \simeq G(0,\omega_0) \simeq 1/[\omega_0 - \epsilon(0)] , \quad (69)$$

in the numerator of Eq. (49), since $\Gamma(\mathbf{p})$ are nonzero only in a small region of the Brillouin zone ($\mathbf{p} < k_0$). Setting $\omega_1 = \omega_2 = \omega_0$, $\eta = 0$ in Eq. (A2) and using the inequality $-2\,\mathrm{Im}\Sigma(\omega_0) \gg \gamma(\omega_0)$, we have

$$L(0,\omega_0,\omega_0) = \frac{1}{M}\sum_{\mathbf{p}}|G(\mathbf{p},\omega_0)|^2 = U_0^{-2} . \quad (70)$$

Substituting Eq. (70) into Eq. (55) and using the sum rule Eq. (20), we obtain

$$\gamma_r(\omega_0) \simeq \frac{U_0^2\gamma_0}{[\omega_0 - \epsilon(0)]^2} . \quad (71)$$

Using Eqs. (68) and (38), we have

$$\frac{\pi D(\omega_0,\omega_0)\rho(\omega_0)}{8a^2} \leq \frac{1}{32\pi}\ln\{2\pi\rho(\omega_0)[\omega_0 - \epsilon(0)]^2/\gamma_0\} . \quad (72)$$

Note that the rhs of Eq. (72) approaches a constant in the weak disorder limit. Since $\rho(\omega_0) \sim W^{-1}$, $\gamma_0 \sim W(k_0a)^3$ [due to Eq. (21)] and putting $|\omega_0 - \epsilon(0)| \sim W$, we can recast Eq. (72) in the form

$$f_0^{-1} \equiv \frac{\pi D(\omega_0,\omega_0)\rho(\omega_0)}{8a^2} \leq \frac{1}{32\pi}\ln\left[\frac{2\pi}{(k_0a)^3}\right] , \quad (73)$$

and for $k_0a \sim 2\pi \times 10^{-3}$ we obtain

$$f_0^{-1} \equiv \frac{\pi D(\omega_0,\omega_0)\rho(\omega_0)}{8a^2} \leq 0.2 . \quad (74)$$

All our results are obtained in the weak disorder limit $f_0 \ll 1$. Equation (74) implies that effects of strong exciton localization, though in principle present for any disorder strength, cannot be observed in practice for weak disorder due to the finite radiative lifetime. In particular, the decrease of the diffusion coefficient, which can show up in the form of backsattering peak, is a very small effect, as illustrated in Fig. 5, which shows that $D_r \simeq D$.

In conclusion, we have shown that for a two-dimensional molecular aggregate with weak disorder, the localization length is always much larger than the mean free path associated with radiative damping. In order to observe effects of strong exciton localization in two-dimensional molecular aggregates, one should go to the region of strong disorder. We expressed the backscattering signal in terms of the exciton diffusion coefficient, which is calculated using the ladder diagram approximation and the renormalization-group technique.

APPENDIX A: THE LADDER AND MAXIMALLY CROSSED DIAGRAM APPROXIMATION FOR THE p-h GREEN FUNCTION

In this appendix, we derive expressions for the p-h Green function ϕ, including ladder and maximally crossed diagrams. Using the perturbating scheme for weak Gaussian diagonal disorder (see, for example, Ref. 27) and taking into account the ladder and the maximally crossed diagrams only, we obtain Eq. (31) with ϕ_c, ϕ_I, and ϕ_{bs} given in Eqs. (33), (40), and (61), and the diffusion propagator $\mathcal{D}$ is given in Eq. (42). Note that the sum of maximally crossed diagrams can be obtained from the sum of ladder diagrams.[23] To obtain Eq. (44) we first put $q = 0$. Integrating the identity

$$G(\mathbf{p},\omega_1) - G^*(\mathbf{p},\omega_2) = [\omega_2 - \omega_1 + \Sigma(\omega_1) - \Sigma^*(\omega_2)$$
$$- 2i\Gamma(\mathbf{p})]G(\mathbf{p},\omega_1)G^*(\mathbf{p},\omega_2) , \quad (A1)$$

over $\mathbf{p}$, making use of Eq. (37), we obtain

$$\Sigma(\omega_1) - \Sigma^*(\omega_2) = U_0^2 L(0;\omega_1,\omega_2)$$
$$\times[-\omega_{12} + \Sigma(\omega_1) - \Sigma^*(\omega_2)$$
$$- i\gamma(\omega_1,\omega_2)] , \quad (A2)$$

where $L(0;\omega_1,\omega_2)$ and $\gamma(\omega_1,\omega_2)$ are defined in Eqs. (43) and (46). Substituting Eq. (A2) into Eq. (42), we obtain Eq. (44) for $q = 0$. Expanding $L(\mathbf{q},\omega_1,\omega_2)$ in Eq. (42) in powers of q to second order,[29] we finally obtain Eq. (44) for small q, where the diffusion coefficient is given by Eq. (45).

APPENDIX B: SUM RULES FOR RADIATIVE DECAY

In this appendix, we derive Eqs. (50) and (51). We use spherical coordinates with the z axis normal to the lattice plane, and assume $\hat{\kappa} = (1,\theta_0,\varphi_0)$, and $\hat{R} = (1,\theta,\varphi)$, where $\hat{\kappa}$ and $\hat{R}$ are the direction of incident and scattered field. Since $\mathbf{k}'$ and $\mathbf{k}$ are the projections of $k_0\hat{R}$ and $k_0\hat{\kappa}$ in the lattice plane ($k_0 = \Omega/c$), we have

$$\delta(\mathbf{k}' - \mathbf{k}) \rightarrow \frac{\delta(k_0\sin\theta_0 - k_0\sin\theta)\delta(\varphi_0 - \varphi)}{k_0\sin\theta_0} . \quad (B1)$$

Using Eqs. (34) and (B1) and the relation

$$\sum_{\mathbf{e}_2}(\mathbf{e}_2\cdot\boldsymbol{\mu})^2 = \mu^2 - (\boldsymbol{\mu}\cdot\hat{R})^2 , \quad (B2)$$

we have

$$\int d\hat{R} \sum_{e_2} \int dt (e_2 \cdot \mu)^2 S_c(t)$$

$$= \frac{8\pi^3}{a^2 k_0^2 |\cos\theta_0|} [2\mu^2 - (\mu \cdot \hat{\kappa})^2 - (\mu \cdot \hat{\kappa}_r)^2]$$

$$\times \int d\omega_0 |G(\mathbf{k}, \omega_0) E(\omega_0)|^2 , \qquad (B3)$$

where $\hat{\kappa}$ and $\hat{\kappa}_r$ are the transmitted and reflected direction, $\hat{\kappa} = \hat{\kappa}^\parallel + \cos\theta_0 \hat{z}$, $\hat{\kappa}_r = \hat{\kappa}^\parallel - \cos\theta_0 \hat{z}$. Using Eq. (18), we get Eq. (50). The total reflected and transmitted coherent signal can be obtained from Eq. (B3) by replacing the term in square brackets by $[\mu^2 - (\mu \cdot \hat{\kappa}_r)^2]$ and $[\mu^2 - (\mu \cdot \hat{\kappa})^2]$, respectively, resulting in Eq. (56).

Substituting Eq. (41) into the left-hand side of Eq. (51), we obtain

$$\int d\hat{R} \sum_{e_2} \int dt (e_2 \cdot \mu)^2 S_I(t) = 2\pi \int d\omega |G(\mathbf{k}, \omega) E(\omega)|^2 \int d\hat{R} [\mu^2 - (\mu \cdot \hat{R})^2] \times |G(\mathbf{k}', \omega)|^2 U_0^2 [-2 \operatorname{Im}\Sigma(\omega) + \gamma(\omega)] / \gamma(\omega)$$

$$= 2\pi \int d\omega |G(\mathbf{k}, \omega) E(\omega)|^2 \int d\hat{R} [\mu^2 - (\mu \cdot \hat{R})^2] |G(\mathbf{k}', \omega)|^2$$

$$\times \frac{-\operatorname{Im}\Sigma(\omega)}{(2\pi)^{-2} a^2 \int d\mathbf{p} \, \Gamma_r(\mathbf{p}) |G(\mathbf{p}, \omega)|^2} \frac{\gamma_r(\omega)}{\gamma(\omega)} . \qquad (B4)$$

We have used Eq. (A2). Both $\mathbf{k}'$ and $\mathbf{p}$ in the above equation are confined in a small region $k' < k_0$ and $p < k_0$, and $|G(\mathbf{p}, \omega)|^2$ change very little in this region. We thus approximate it by a constant. Thus $|G(\mathbf{k}', \omega)|^2$ and $|G(\mathbf{p}, \omega)|^2$ in the above equation cancel. Using the sum rule Eq. (20) and the relation

$$\int d\hat{R} [\mu^2 - (\mu \cdot \hat{R})^2] = \frac{8\pi}{3} , \qquad (B5)$$

we finally obtain Eq. (51).

APPENDIX C: LOW-FREQUENCY ASYMPTOTICS OF THE DIFFUSION PROPAGATOR

In this appendix, we derive an expression for the diffusion propagator in the low-frequency (infrared) regime [Eq. (63)]. As indicated in Sec. V, the diffusion propagator D can be treated as a two point correlation function in the nonlinear sigma model (see Ref. 22). The parameters of this model are the dimensionless inverse diffusion coefficient defined as follows (we will use notation of Ref. 22 except that t is replaced by f to avoid confusion with the time variable):

$$f_0 \equiv \frac{8a^2}{\pi D(\omega_0, \omega_0) \rho(\omega_0)} , \qquad (C1)$$

and $\gamma(\omega_0) - i\omega_{12}$. In the weak disorder limit, the renormalization-group equations describe the scaling properties of the parameters. The parameter $\gamma(\omega_0) - i\omega_{12}$ as well as the Green function itself are not renormalized, which is a consequence of the supersymmetry. The equation for $f(\xi)$ has the form[22]

$$\frac{d\tilde{f}}{d \ln \xi} = -\tilde{f}^2 , \quad \tilde{f} \equiv \frac{f}{16\pi} , \quad f(\xi) \ll 1 , \qquad (C2)$$

where ξ is the scaling parameter. It follows from Eq. (C2) that in the region $f(\xi) \ll 1$, the renormalized diffusion coefficient $D_r(\mathbf{q}; \omega_1, \omega_2)$ for small q and ω_{12} depends on the renormalized parameter:

$$f(\Lambda) \equiv \frac{8a^2}{\pi D_r(\mathbf{q}, \omega_1, \omega_2) \rho(\omega_0)} , \qquad (C3)$$

$$\frac{1}{f(\Lambda)} = \frac{1}{f_0} - \frac{1}{32\pi} \ln(\Lambda_0/\Lambda)^2 . \qquad (C4)$$

Λ_0 is the high-frequency cutoff, which is the momentum-space scale where the renormalization of the diffusion coefficient becomes important, i.e.,

$$\Lambda_0^2 = [D(\omega_0, \omega_0) \tau(\omega_0)]^{-1} . \qquad (C5)$$

The parameter Λ generally speaking depends on q and $\gamma(\omega_0) - i\omega_{12}$. To obtain this dependence we can use the result of perturbative calculation of the transverse Green function in the sigma model[22] which leads to the following definition of Λ:

$$\Lambda^2 = \frac{\gamma(\omega_0) - i\omega_{12}}{D(\omega_0, \omega_0)} . \qquad (C6)$$

Combining Eqs. (C4)–(C6), we obtain

$$\frac{1}{f} = \frac{1}{f_0} - \frac{1}{32\pi} \ln \left\{ \frac{1}{[\gamma(\omega_0) - i\omega_{12}] \tau(\omega_0)} \right\} . \qquad (C7)$$

Substituting f from Eq. (C7) into Eq. (C3), we obtain the renormalized diffusion coefficient. Substituting it instead of the bare diffusion coefficient into Eq. (44), we obtain the expression of Eqs. (63) and (64) for the diffusion propagator.

Note that Eq. (C6) is valid in the region $D(\omega_0, \omega_0) q^2 \sim \gamma(\omega_0)$, i.e., in the region of the peak. Equation (C6) leads to the form of the renormalized diffusion coefficient being independent on the momentum q. This breaks down for $D(\omega_0, \omega_0) q^2 \gg \gamma(\omega_0)$, but in this region the value of the backscattering signal is small.

*Also at Department of Physics, University of Rochester, Rochester, NY 14627.

†Also at Institute of Spectroscopy, Russian Academy of Sciences, Troitsk, Moscow Region 142092, Russia.

[1] F. C. Spano, J. R. Kuklinski, and S. Mukamel, J. Chem. Phys. 94, 7534 (1991); Phys. Rev. Lett. 65, 211 (1990); F. C. Spano and S. Mukamel, J. Chem. Phys. 91, 683 (1989).

[2] D. Mobius and H. Kuhn, Isr. J. Chem. 18, 375 (1979); J. Appl. Phys. 64, 5138 (1988).

[3] S. Deboer and D. A. Wiersma, Chem. Phys. Lett. 165, 45 (1990); S. Deboer, K. J. Vink, and D. A. Wiersma, ibid. 137, 99 (1987).

[4] A. A. Muenter et al., J. Phys. Chem. 96, 2783 (1992).

[5] F. C. Spano et al., Mol. Cryst. Liq. Cryst. 194, 331 (1991).

[6] H. Fidder, J. Knoester, and D. A. Wiersma, J. Chem. Phys. 95, 7880 (1991).

[7] T. Tani, T. Suzumoto, K. Kemnitz, and K. Yoshihara, J. Phys. Chem. 96, 2778 (1992).

[8] V. M. Agranovich, Zh. Eksp. Teor. Fiz. 37, 430 (1959) [Sov. Phys. JETP 10, 307 (1960)].

[9] M. Oritt, C. Aslangul, and Ph. Kottis, Phys. Rev. B 25, 7263 (1982); M. Orrit and Ph. Kottis, Adv. Chem. Phys. 74, 1 (1988).

[10] J. J. Hopfield, Phys. Rev. 112, 1555 (1988).

[11] M. R. Philpott, J. Chem. Phys. 52, 5842 (1970).

[12] V. M. Agranovich and O. Dubovsky, Zh. Eskp. Teor. Fiz. 3, 345 (1966) [Sov. Phys. JETP 3, 223 (1966)].

[13] J. K. Jenkins and S. Mukamel, J. Chem. Phys. 98, 7046 (1993).

[14] V. Chernyak and S. Mukamel, Phys. Rev. B 48, 2470 (1993).

[15] V. Chernyak and S. Mukamel, J. Chem. Phys. 100, 2953 (1994).

[16] N. Wang, V. Chernyak, and S. Mukamel, J. Chem. Phys. 100, 2465 (1994).

[17] N. Wang, J. K. Jenkins, V. Chernyak, and S. Mukamel, Phys. Rev. B (to be published).

[18] N. Wang, A. A. Muenter, and S. Mukamel, J. Chem. Phys. 99, 3604 (1993).

[19] H. P. van Albada and A. Lagendijk, Phys. Rev. Lett. 55, 2692 (1985); E. Akkermans, P. E. Wolf, and R. Maynard, ibid. 56, 1471 (1986); A. A. Golubentsev, Zh. Eskp. Teor. Fiz. 86, 47 (1984) [Sov. Phys. JETP 59, 26 (1984)].

[20] V. E. Kravtsov, V. I. Yudson, and V. M. Agranovich. Phys. Rev. B 41, 2794 (1990).

[21] V. M. Agranovich, V. Ya Chernyak, K. I. Grigorishin, and E. I. Ogievetsky, Phys. Lett. A 165, 289 (1992).

[22] K. B. Efetov, Adv. Phys. 32, 53 (1983).

[23] D. Vollhardt and P. Wölfle, Phys. Rev. Lett. 45, 842 (1980); Phys. Rev. B 22, 4666 (1980).

[24] A. S. Davydov, Theory of Molecular Excitons (Plenum, New York, 1971).

[25] L. Mower, Phys. Rev. 142, 799 (1966).

[26] M. L. Goldberger and K. M. Watson, Collision Theory (Wiley, New York, 1969).

[27] A. A. Arbikosov, L. P. Gorkov, and I. E. Dzyaloshinski, Methods of Quantum Field Theory in Statistical Physics (Dover, New York, 1975).

[28] J. Kroha, Physica A 167, 231 (1990).

[29] N. Wang, J. A. Leegwater, and S. Mukamel, J. Chem. Phys. 98, 5899 (1993).

[30] E. N. Economou, Green's Functions in Quantum Physics (Springer-Verlag, New York, 1983).

[31] L. Van Hove, Phys. Rev. 89, 1189 (1953); H. P. Rosenstock, ibid. 97, 290 (1955).